Chapter 8: Viscosity and Flow Laws

THE GLOBAL flow in rocks, deforming by dynamic recrystallization, is accommodated by diffusion creep, dislocation creep, or superplasticity, or a combination of these processes. The strain memory of the granular texture of the rocks is limited, but it is necessarily disregarded in a simple continuum approach. What matters is the macroscopic deformation, the statistical average of all microscopic displacements as can be seen from passive strain markers, in contrast to the active boundary migration of recrystallizing grains. This chapter completes the introduction to rock rheology and concentrates on practical measures and expressions for quantifying rock flow.

Contents: Section 8-1 defines the quantity of viscosity, and examples are given in section 8-2. Visco-elasticity models for rock deformation are outlined in section 8-3. Non-Newtonian creep, strain softening, and strain-rate softening are discussed in sections 8-4 and 8-5. Flow curves, creep laws, and lithospheric strength curves are introduced in sections 8-6 to 8-9. Geological applications of lithospheric strength diagrams are outlined in section 8-10.

Practical hint: **A good intuitive understanding of the rheological behavior comprised in the term viscosity can be established using commercially available rheometers on a range of low-viscosity materials, such as oils, syrup, honey, and modeling clays. A visit to a uniaxial or triaxial rig, deforming rock specimens under hot press conditions, can further consolidate the understanding of the physical parameters involved in rock creep.**

8-1 Viscosity

The rate of deformation in crystalline creep by diffusion is proportional to the applied stress, similar to that observed in moving fluids. The proportionality constant is termed the *viscosity*, which is a measure for the ductility (or *"flow resistance"*) of the viscous body, moving by simple shear. The shear viscosity is measured by shearing the viscous body between two sub-

parallel platens (Fig. 8-1a). The shear is maintained by pulling the upper platen of surface area, A, with force, F, parallel to the plane of the platen. The deviatoric shear stress, τ (=F/A), on the viscous body and the *velocity gradient*, u/d, or *engineering shear strain-rate*, $\dot{\gamma}$=u/d, are related by the dynamic viscosity, η:

$$\tau=\eta(u/d) \qquad (8\text{-}1)$$

Sir Isaac Newton first postulated this linear relationship between the stress and strain-rate in his book *Mathematical Principles of Natural Philosophy* of 1687. Fluids which obey linearity are, therefore, termed *Newtonian* or *linear*; the strain-rate doubles if the stress is doubled.

The viscosity of viscous bodies tends to be strongly temperature-dependent, resulting in remarkable *thermal softening* in zones of increased heat flow. The viscosity of Newtonian bodies decreases, approximately according to the *Arrhenius relationship*:

$$\eta=A\ \exp(B/T) \qquad (8\text{-}2)$$

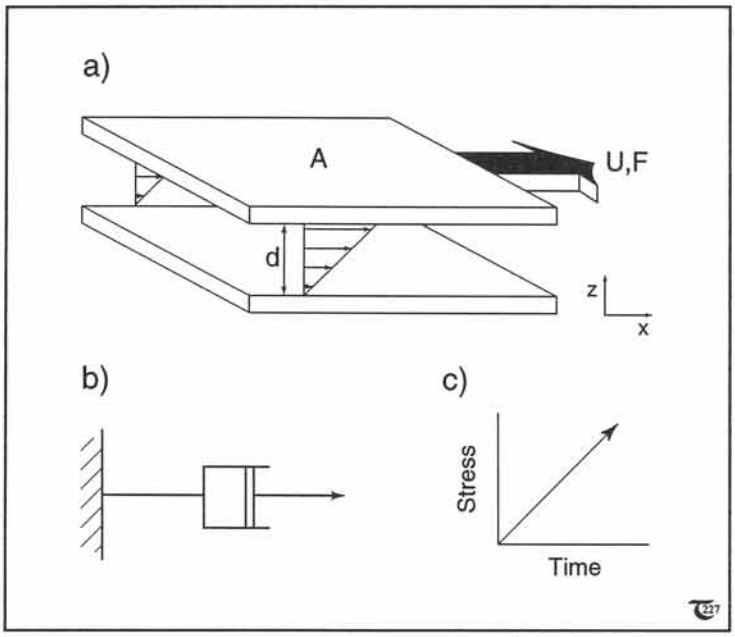

Figure 8-1: *a) Definition sketch for the dynamic viscosity. b) Dashpot as a mechanical anolog for viscous flow. c) Stress-time graph for viscous flow.*

where T is the absolute temperature and A and B are constants of the liquid. Figure 8-2 shows the drop in viscosity with increasing temperature for liquid magma and silicate glasses.

Newtonian shear viscosity, at constant temperature, has the following characteristics: (1) the shear viscosity does not vary with the shear-rate, (2) the viscosity remains constant with time, and (3) the only stress occurring in shear flow is the shear stress; no normal stresses are generated.

☐Exercise 8-1: a) Determine from expression (8-1) in what units the dynamic shear viscosity is expressed. b) Is this viscosity a scalar, vector, or tensor quantity?

8-2 Examples of viscosities

The viscous resistance of Newtonian fluids is usually portrayed by a mechanical *dashpot model* (Figs. 8-1b & c). Viscosity has the dimensions of Pa s, as can be inferred from equation (8-1). Examples of the viscosity of common materials are given in Table 8-1. The viscosity of air is 10^{-5} Pa s, water 10^{-3} Pa s, olive oil 10^{-1} Pa s, honey 10 Pa s, silicone putty 10^{4} Pa s, H_2O-ice 10^{10} Pa s, and rock salt 10^{17} Pa s, all at room temperature. The viscosity of rocks ranges from 10^{20} Pa s for mantle peridotites to 10^{24} Pa s for granites in the lower continental crust. Because of the enormous range of viscosities in natural materials, it is obvious that each particular viscometer, an instrument to measure the viscosity of viscous bodies, is suitable for only a small range of materials.

Apart from the *dynamic shear viscosity* outlined here, other viscosity parameters, measured in flow configurations different from simple shear, are used in fluid mechanics. One example is the *extensional*

Table 8-1: *Dynamic viscosity of common materials.*

Substance	*Pa s*
Air	10^{-5}
Water	10^{-3}
Olive oil	10^{-1}
Honey	10
Silicone gum	10^{4}
Water ice	10^{10}
Rock salt	10^{17}
Peridotite	10^{20}
Granite	10^{24}

viscosity, which is measured sandwiching a stiff liquid between two platens, while allowing for lateral extrusion in all radial directions. The stress is truly uniaxial, and no confining pressure can ever exist in this configuration. Another example of an alternative measure of viscous friction is the *kinematic viscosity*, ν, which is simply related to the dynamic viscosity, η:

$$\nu = \eta/\rho \qquad (8\text{-}3)$$

The kinematic viscosity can be used as a measure for the diffusion of viscous motion away from a perturbation, but it is less commonly applied in mechanical models of rock deformation.

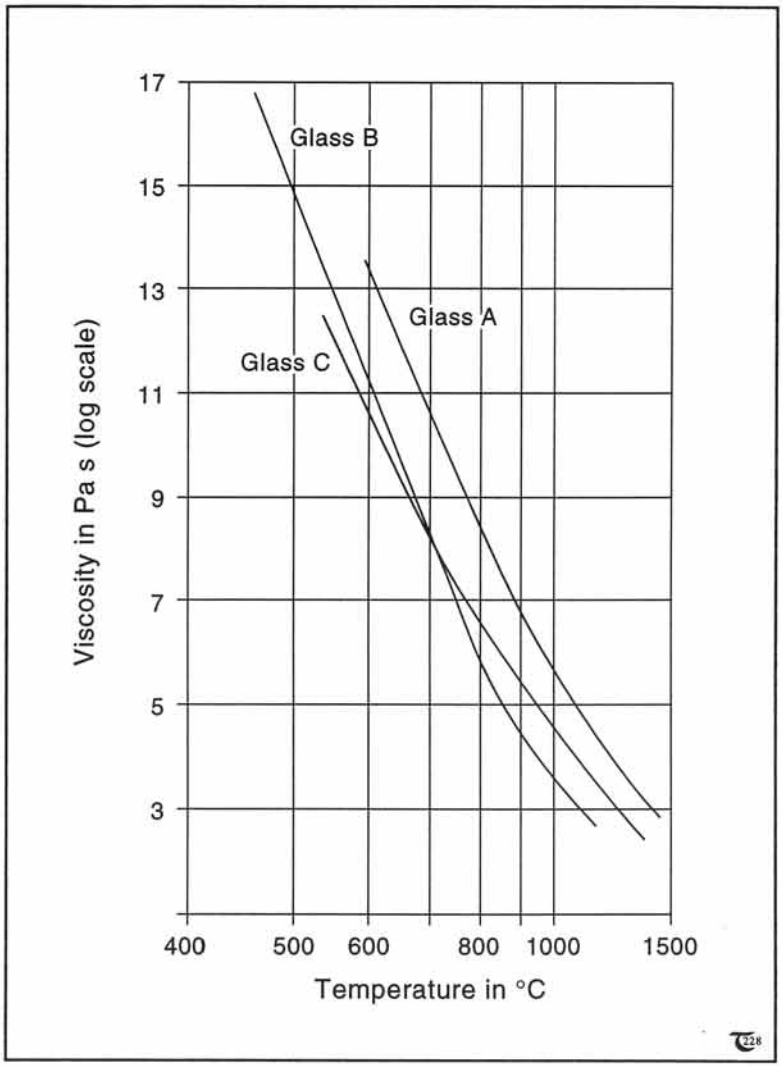

Figure 8-2: *Thermal softening of three different silicate glasses. Glass A has 75% SiO_2, glass B is comprised of 67% SiO_2, and glass C has 72% SiO_2.*

☐Exercise 8-2: a) Establish in what units the kinematic viscosity is expressed. b) Is this viscosity a scalar, vector, or tensor quantity?

☐Exercise 8-3: Examine some real samples of the materials listed in Table 8-1, and test their rheology in a qualitative fashion, in order to develop a good feel for the relative magnitude of their viscosities.

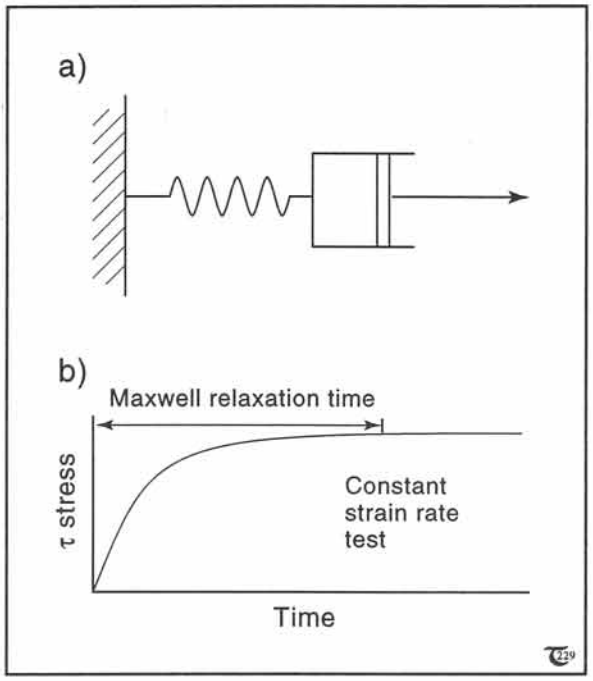

Figure 8-3: a) The Maxwell body portrayed as a mechanical arrangement of a spring and a dashpot. b) Stress-time graph for a typical Maxwell body.

8-3 Visco-elasticity

Rocks deforming at depth should more precisely be considered as visco-elastic bodies, because all rocks, whether shallow or deep in the Earth's crust and mantle, initially respond elastically to any stress at any depth. This behavior is similar to that of a mechanical model, comprising both a dashpot and spring in series: a so-called *Maxwell body* (Fig. 8-3a). The initial reponse is elastic, but that is followed by irreversible ductile flow. The stress-time curve is portrayed in Figure 8-3b. Permanent distortion will occur after the so-called *Maxwell relaxation time*, t_m, has elapsed:

$$t_m = \eta / G \qquad (8\text{-}4)$$

with dynamic viscosity, η, and elastic shear modulus, G. A typical viscosity of crustal rocks is 10^{24} Pa s and a typical shear modulus is 10^{11} Pa, so Maxwell relaxation times for rocks may be some 300,000 years. This explains why elastic depression of the crust by glacial loading, during glacial episodes of less than 300,000 years, will be elastically recovered after cessation of the glaciation. Usually, the crustal rebound is anelastic, due to viscous

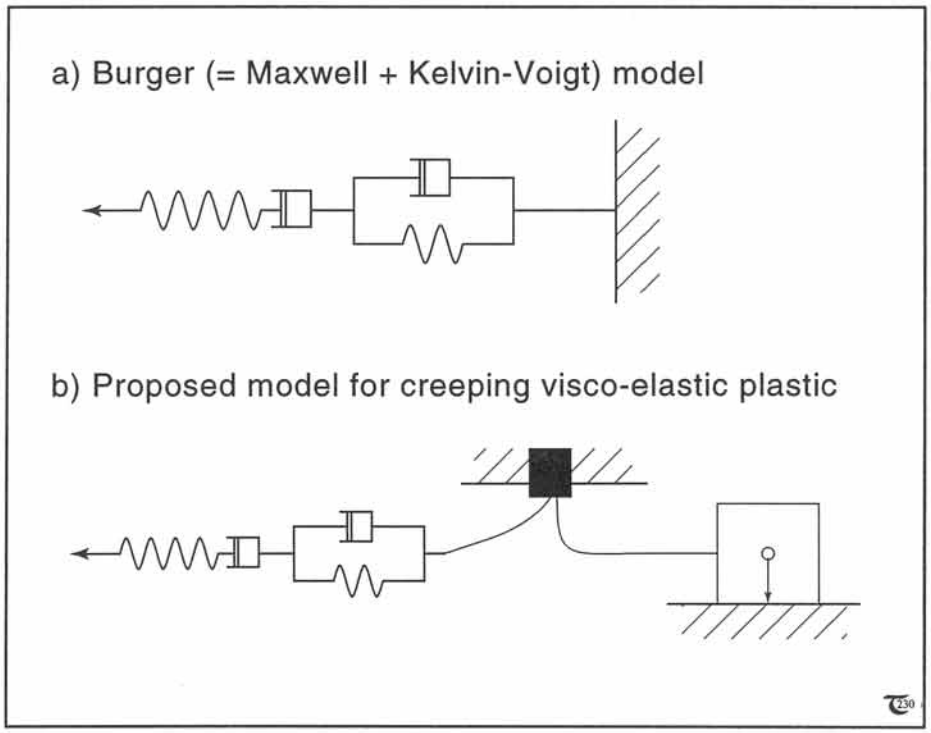

Figure 8-4: a) Mechanical arrangement, simulating the rheology of a Burger body. b) Possible mechanical analog for visco-elastic plastic behavior.

Figure 8-5: Compilation of some major mechanical analog models for elastic, viscous, and viscoelastic behavior. The corresponding graphs for creep tests, constant strain-rate tests, and stress-relaxation tests are shown for each analog model.

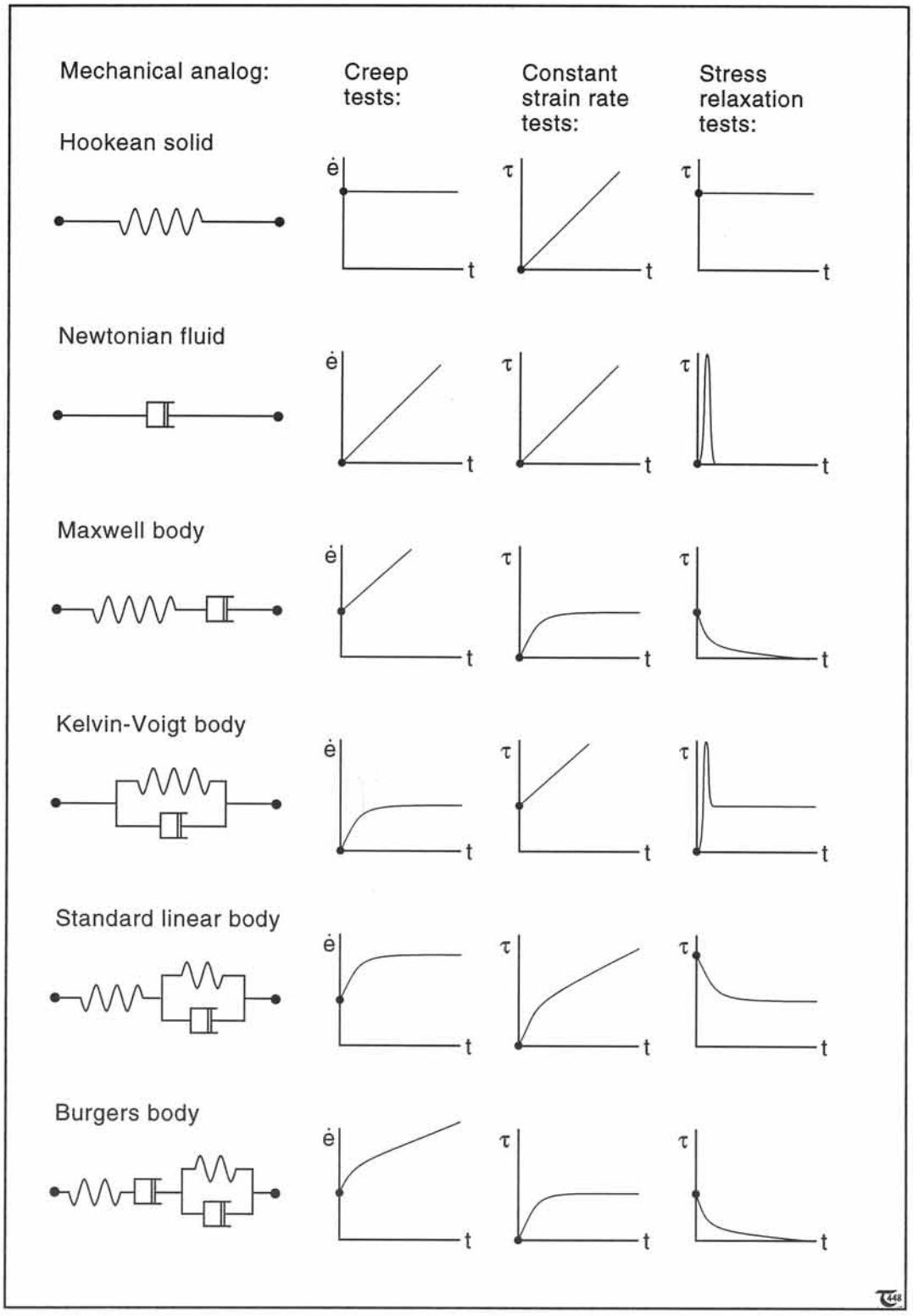
Mechanical analog:
Creep tests:
Constant strain rate tests:
Stress relaxation tests:
Hookean solid
Newtonian fluid
Maxwell body
Kelvin-Voigt body
Standard linear body
Burgers body
ė
τ
t

retardation by the underlying mantle, which has much shorter Maxwell relaxation times, arising from a lower viscosity.

A parameter, closely related to the Maxwell relaxation time, is the *Deborah number*, De, introduced by Marcus Reiner, one of the founders of the science of rheology:

$$De = t_c/t \qquad (8\text{-}5)$$

where t is the time for which the deformation process lasts and t_c a characteristic time of the material, e.g., $t_c = t_m$. The idea is that all matter flows if one were to wait long enough, in accordance with Deborah's observation reported in the Old Testament: *" The mountains flowed before the Lord... ."* Permanent distortion occurs if De is smaller than unity.

The regular visco-elastic mechanical analog can be modified to include anelasticity, combining a

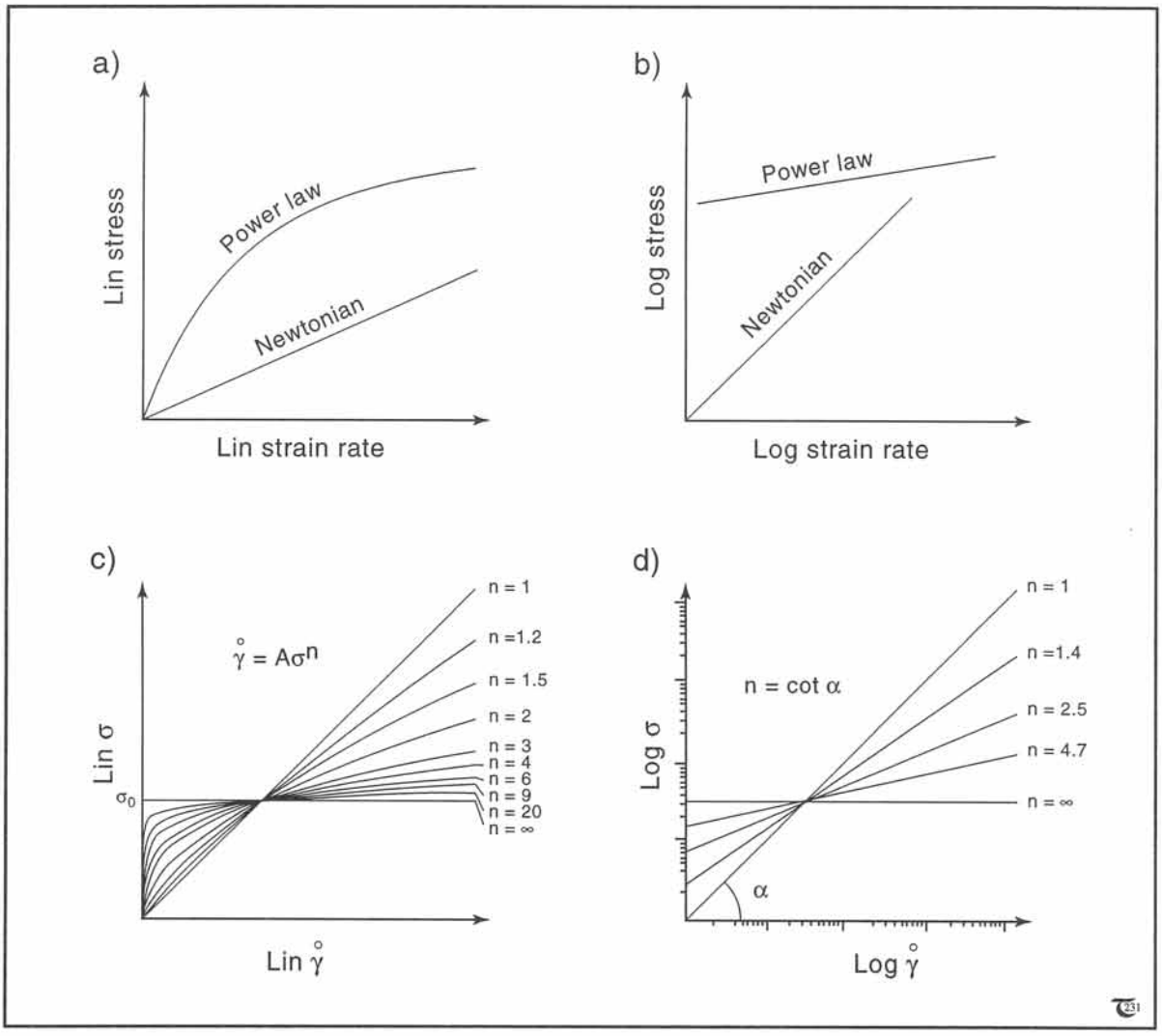

Figure 8-6: *a) to d) Stress - strain-rate graphs for steady-state flow of rocks. Linear coordinate axes are used in graphs (a) and (c); logarithmic axes in (b) and (d). The plots of (a) and (b) are simplified versions of (c) and (d), respectively. See text and exercise 8-5.*

Kelvin-Voigt unit with *Maxwell's unit*, as portrayed in Figure 8-4a. This composite mechanical model is known as a *Burger body*. This mechanical model possibly demonstrates best the rheological behavior of visco-elastic rocks. A model, which could account for both crystal plasticity and failure, followed by frictional plasticity at rapid stress loads, is proposed in Figure 8-4b.

☐Exercise 8-4: Figure 8-5 compiles some of the major mechanical analogs for rheological behavior of visco-elastic materials and rocks. The corresponding curves, typical for creep tests, constant strain-rate tests, and stress-relaxation tests, are, also, given for each type of behavior. Examine each of the the three types of graphs. Now decide which type of rheological test best allows the classification of a material uniquely as fitting one of the mechanical analog models.

8-4 Non-Newtonian creep

Rocks flow as Newtonian bodies only if deforming by *diffusion creep mechanisms*. The global flow of rocks, deforming by *dislocation creep mechanisms*, does not obey the linear behavior suggested by Newton for viscous bodies (Figs. 8-6a & b). Instead, the deformation rate is related to the applied shear stress, τ, by a power law, according to:

$$\tau^n = A\dot{\gamma} \qquad (8\text{-}6)$$

with material constant, A, expressed in units of Pa^n s, power, n, and engineering strain-rate, $\dot{\gamma}$. The power factor, n, varies for rocks between 1 and 10. It is convenient to plot these power-law functions in *log stress-log strain-rate* space, because they appear as straight lines with slope, α, equal to $\cot^{-1}n$ (Figs. 8-6c & d). The exponent of Newtonian rocks is unity, and flow by dislocation creep occurs for n larger than unity ($n > 1$).

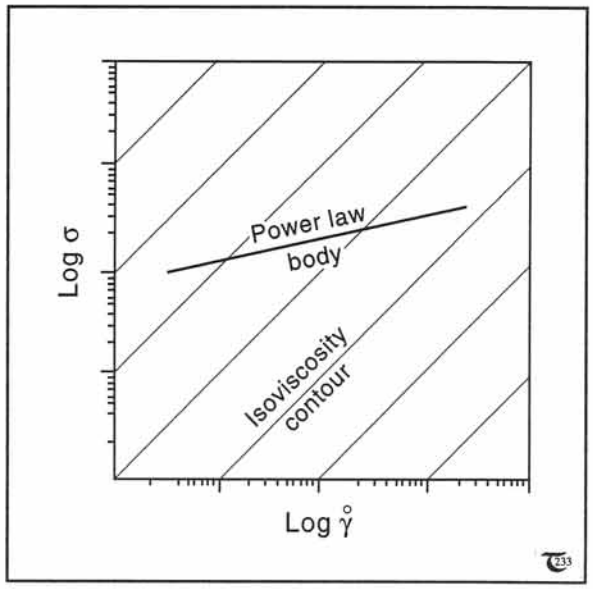

Figure 8-7: *The diagonals in log stress-log strain-rate space correspond to iso-viscosity contours, provided that both axes are positive and scaled with similar spacing.*

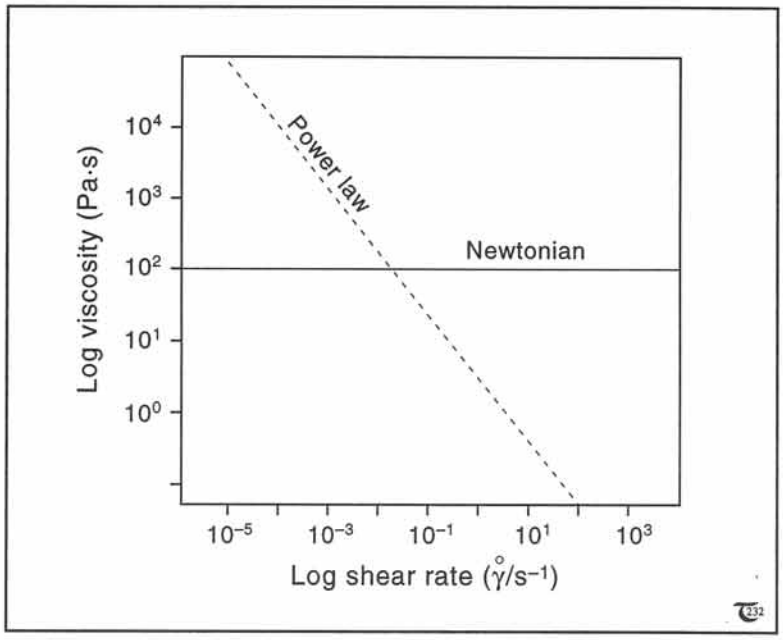

Figure 8-8: *General graph of viscosity dependence on the strain rate for Newtonian and power-law substances.*

Figure 8-7 illustrates how iso-viscosity contours can be plotted in *log stress-log strain-rate* space. The viscosity of rocks in power-law flow characteristically is dependent of the shear strain-rate (Fig. 8-8). Only an effective viscosity can be defined, according to:

$$\eta_{eff} = \tau_c / \dot{\gamma}_c = A^{1/n} \dot{\gamma}_c^{(1/n)-1} \qquad (8\text{-}7)$$

It follows from equation (8-7) that a small increase in the strain-rate results in a rapid decrease of the effective viscosity, provided n is larger than unity. Power-law bodies may have effective viscosities, covering a range of several orders of magnitude, according to the variation of the strain-rate that deforms them. A power-law, viscous body can, also, be referred to as *shear-rate thinning* or *strain-rate softening* material.

☐Exercise 8-5: Determine n-values for the power-law body in Figure 8-8.

☐Exercise 8-6: Plot the effective viscosity of a granite, using equation (8-7) with $A = 10^{24}$ Pa^n s, strain-rates ranging between 10^{-10} and 10^{-15} s^{-1}, and n-values of 1, 2, and 10.

8-5 Strain softening and strain-rate softening

It is important to distinguish carefully between strain-rate softening behavior and *strain softening*. Strain-rate softening is a general flow characteristic, established by subjecting a viscous body to a range of *steady-state* strain-rates. Strain softening is time-dependent softening of a body, while prohibiting the maintenance of a constant stress or strain-rate. These rates must change due to structural changes of the internal fabric. Consequently, the continuum assumption for strain softening bodies is more complex, or less practical, than that for strain-rate softening bodies. *Strain hardening* bodies show a time-dependent hardening, which does occur in rocks when the grain size increases, during diffusion creep. However, *strain-rate hardening* is not likely to exist for any material, as it would imply that an increase in strain-rate, after reaching steady-state, would result in an effective viscosity higher than at the previously lower steady-state strain-rate.

☐Exercise 8-7: a) Draw a qualitative *log stress-log strain-rate* graph, including examples of hypothetical flow curves for strain-rate softening and strain-rate hardening flow. b) Explain the problem of energy balance in strain-rate hardening.

8-6 Laboratory constraints of flow

To determine flow curves for rocks and minerals, most common laboratory experiments apply a series of particular constant strain-rates to the sample and measure the change of differential stress as the strain progresses. One particular strain-rate yields only one particular deviatoric stress in steady state, as has been discussed in section 7-3. Flow curves of crystalline (usually monomineralic) rocks have been measured at high confining pressures and temperatures, corresponding to those expected at the natural depths where the rocks flow. For example, polycrystalline olivine is deformed at subcrustal temperatures in excess of 1,200 K and confining pressure of 1,000 MPa. Polycrystalline rock salt or halite occurs at natural depths between the surface and 15 km (Fig. 8-9a), and the flow curves have been measured, therefore, at 0 to 200 MPa confining pressure and temperatures of 300 to 700 K.

Measured steady-state flow data are available for laboratory strain-rates between 10^{-9} s^{-1}, and 10^{-2} s^{-1}. At strain-rates faster than 10^{-2} s^{-1} the jackets sealing the samples fail before steady-state creep is attained, and the measurements include

Figure 8-9a: *Ductile flow folds in sedimentary sequence of dirty rock salt around a salt plug in the Great Kavir basin, northern Iran.*

Figure 8-9b: *Flow of ice glacier with dark flow bands, due to lateral moraines. Shallow crevasses in the surface indicate that the brittle-ductile transition lies just beneath the ice surface.*

only elastic effects. On the other hand, measurements at strain-rates slower than 10^{-9} s^{-1} require experiments over impractically long periods of years. Natural strain-rates in rocks generally vary between 10^{-15} and 10^{-13} s^{-1}. Rock salt is unusually soft and may flow in nature at subsurface strain-rates of up to 10^{-8} s^{-1}. Strain-rates measured in spreading ice sheets are in the order of 10^{-11} s^{-1}, but they may speed up to 10^{-7} s^{-1} in glaciers (Fig. 8-9b). Strain-rates below 10^{-20} s^{-1} certainly have no geological significance, because such rates could establish only an infinitesimally small strain, of 0.001 within the 4.5 Ga (10^{17} s) of Earth's history.

The flow regimes of rocks at natural strain-rates on the order of 10^{-14} s^{-1} have been estimated by extrapolation of laboratory data and theoretical arguments. For example, ductile flow, under the relatively fast laboratory strain-rates at laboratory conditions, is almost exclusively occurring by dislocation creep mechanisms. But the calculation

☐Exercise 8-8: a) Examine Figure 8-10 and indicate the appropriate numbers along the viscosity scale. b) What is the viscosity of 243 Kelvin ice, flowing at 10^{-11} s^{-1}? c) What is the effective viscosity for this ice when flowing at 10^{-7} s^{-1}?

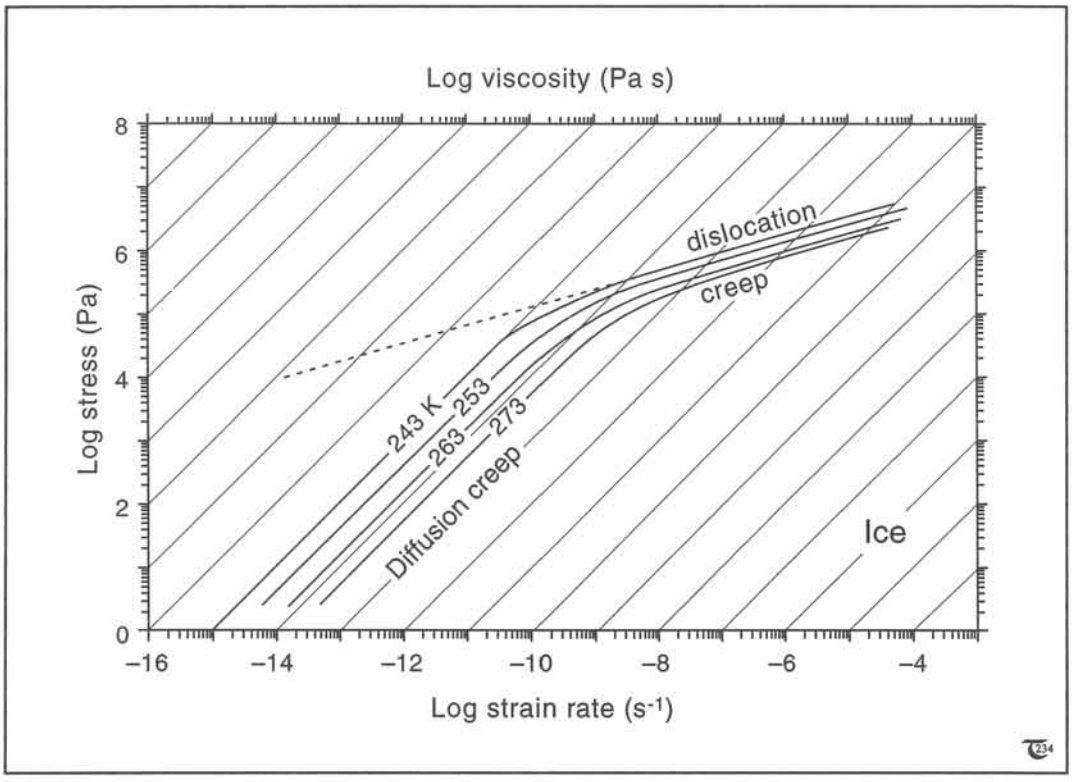

Figure 8-10: *Creep curves for ice at temperatures of 243, 253, 263 and 273 Kelvin. Dislocation creep dominates in the regime of power-law flow at faster strain-rates. Diffusion creep is Newtonian and dominates at slower strain-rates. Because the flow is assumed in steady-state, the average grain size remains constant during flow.*

of flow laws from diffusion creep coefficients suggests that, at least, some rocks can deform by diffusion creep at the much slower strain-rates occurring in nature with less stress input than required for dislocation creep. Figure 8-10 illustrates that ice creeping at strain-rates between 10^{-11} and 10^{-12} s^{-1} deforms by diffusion creep, because the effective viscosity in diffusion creep, within this range of strain-rates, is lower than that for dislocation creep. The effective viscosity of rocks is generally lower at higher strain-rates.

8-7 Creep laws

The flow behavior of rocks can be concisely represented by the following *constitutive creep law*:

$$\dot{e}_1 = A \exp(-Q/RT)(\sigma_1-\sigma_3)^n \quad (8\text{-}8a)$$

which can be rearranged as follows:

$$(\sigma_1-\sigma_3) = (\dot{e}_1/A)^{1/n}\exp(Q/nRT) \quad (8\text{-}8b)$$

with differential stress or strength, $(\sigma_1-\sigma_3)$, normal principal strain-rate, $\dot{e}_1$, activation energy, Q, material constant, A, stress exponent, n, Boltzmann's gas constant, R (=8.315 J K^{-1} mol^{-1}), and temperature, T(K)= T_o(K)+ζz(km); T_o is the surface temperature, and ζ the geotherm in K/km. What is determined in the laboratory tests on rock rheology are the flow parameters A and n. Expressions (8-8a & b) can be modified, using deviatoric stress (τ_1), instead of the differential stress $\sigma_1-\sigma_3$ ($=2\tau_1$), but the form employed here allows direct comparison with brittle failure envelopes, expressed in terms of differential stress.

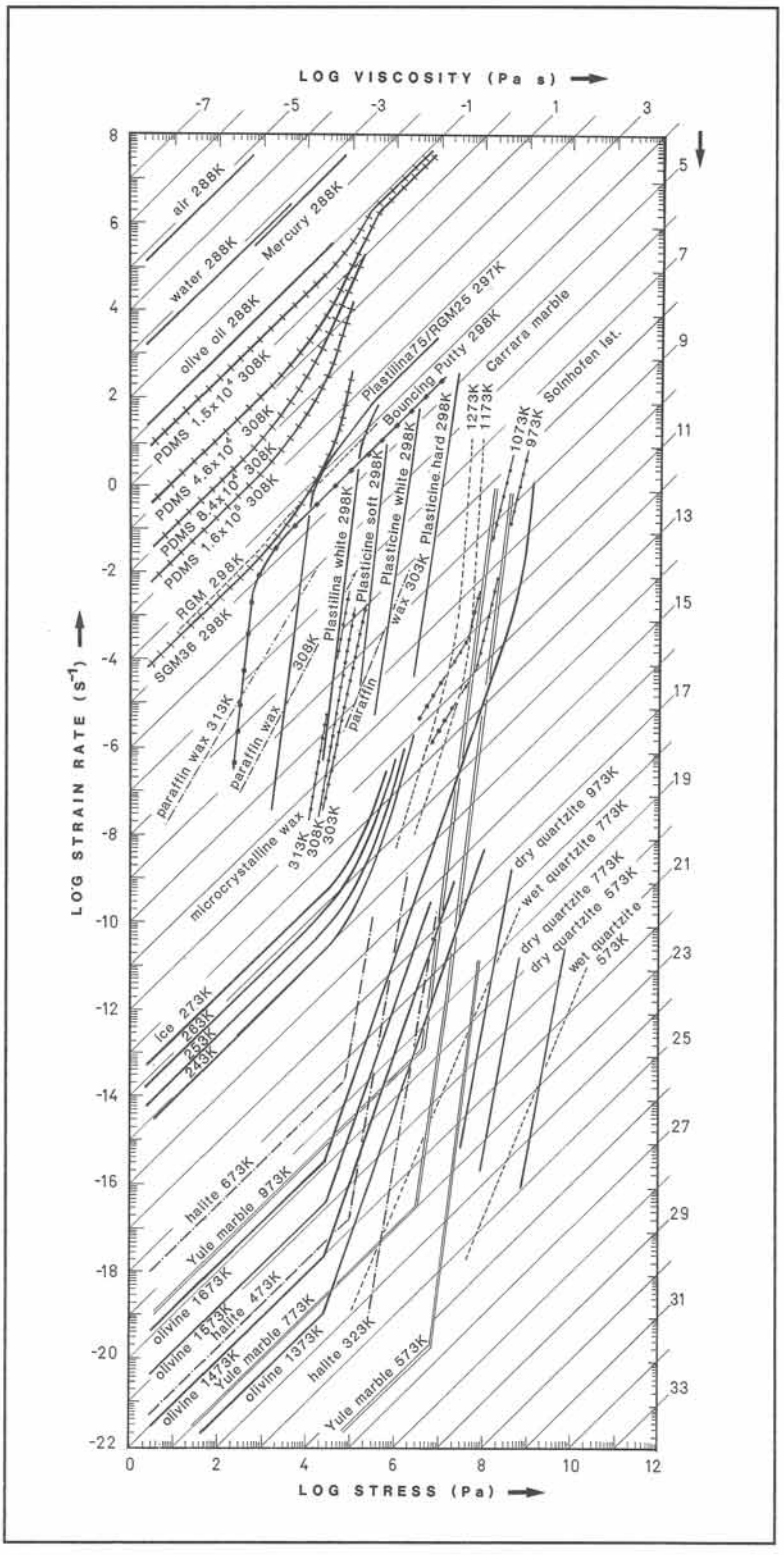

Figure 8-11: Viscosity window for a range of synthetic and natural materials. Logarithmic exponents of ground number 10.

Table 8-2: Steady-state flow parameters for common rocks.

Rock	Log A ($MPa^{-n}s^{-1}$)	n	Q ($kJ\ mol^{-1}$)
Ice (240-258 K)	11.8	4	91
Rock salt	-5.4	4.9	50.2
Dry quartzite	9	2	167
Wet quartzite	10.4	2.4	160
Marble	48.6	7.6	418
Granite	8.5	2.9	106
Diorite	11.5	2.4	219
Diabase	17	3.4	260

Figure 8-11 compiles some flow curves for a variety of monomineralic rocks in *log stress-log strain-rate* space. The plot includes flow curves for some well-known fluids and materials commonly used in analog scale models to give a feel for the astronomical numbers involved in solid rock rheology. The deviatoric stresses characteristic of tectonic deformations are generally assumed to lie in the range of 10 to 100 MPa. Table 8-2 compiles the material constants, A, and stress exponents, n, for a range of rock types and minerals.

In order to be able to describe the rheological behavior of rocks, it is necessary to apply the description to volumes, which remain texturally and compositionally unchanged during the deformation. *Time-dependent rheology*, accounting for compositional and textural changes, is rather complex, and our present knowledge of rock flow allows only a very simplistic approach. This implies that current constitutive equations cannot account for compositional changes, textural changes, or time-dependent volume changes. The limitations of this simplistic continuum model are severe for the creeping flow of rock, where time scales involved are much larger than those of instantaneous elastic distortion or brittle faulting.

☐Exercise 8-9: Calculate and plot the flow curves in *log stress-log strain-rate* space for some of the rocks listed in Table 8-2.

8-8 Thermal softening and hydro-softening

Equation (8-8b) can, also, be used to plot the temperature dependence of rock rheology. Figure 8-12 graphs the temperature dependence of the rock strength for a variety of rocks. The differential stress indicated is that required to maintain ductile creep at a steady strain-rate of $10^{-14}\ s^{-1}$. The temperature in the crust increases with depth, and the temperature scale of Figure 8-12, therefore, can be scaled for depth if the local geothermal gradient is known. The important conclusion of the compilation in Figure 8-12 is that rock strength decreases exponentially with depth.

The effective viscosity of a rock is dependent not only on the lithology, temperature, and strain-rate, but it, also, is greatly influenced by the presence of thin fluid films between the grain boundaries. *Hydro-softening*, a term introduced here for practical purposes, operates if fluid films are present, enhancing diffusion creep mechanisms and, thereby, reducing the effective viscosity of rocks. For example, Joffé had already noted in 1925 that the presence of brine has a profound softening effect upon the rheology of rock salt: the *Joffé effect*. We now know that the amount of intercrystalline brine required for activating diffusion creep is extremely low, about 0.05 wt%. Because most natural rock salts contain 0.1 to 1.0 wt% intercrystalline brine, they may be considered sufficiently wet to allow diffusion or solution-transfer creep. In rock salt, diffusion (linear) creep will usually dominate over simultaneous dislocation (power-law) creep at the low strain-rates characteristic of geologic deformations.

☐Exercise 8-10: Consider interleaving quartzite and marble layers, deforming at 200° centigrade. Consult Figure 8-12 to decide which layers will buckle upon layer-parallel-shortening, the quartzites or the marbles?

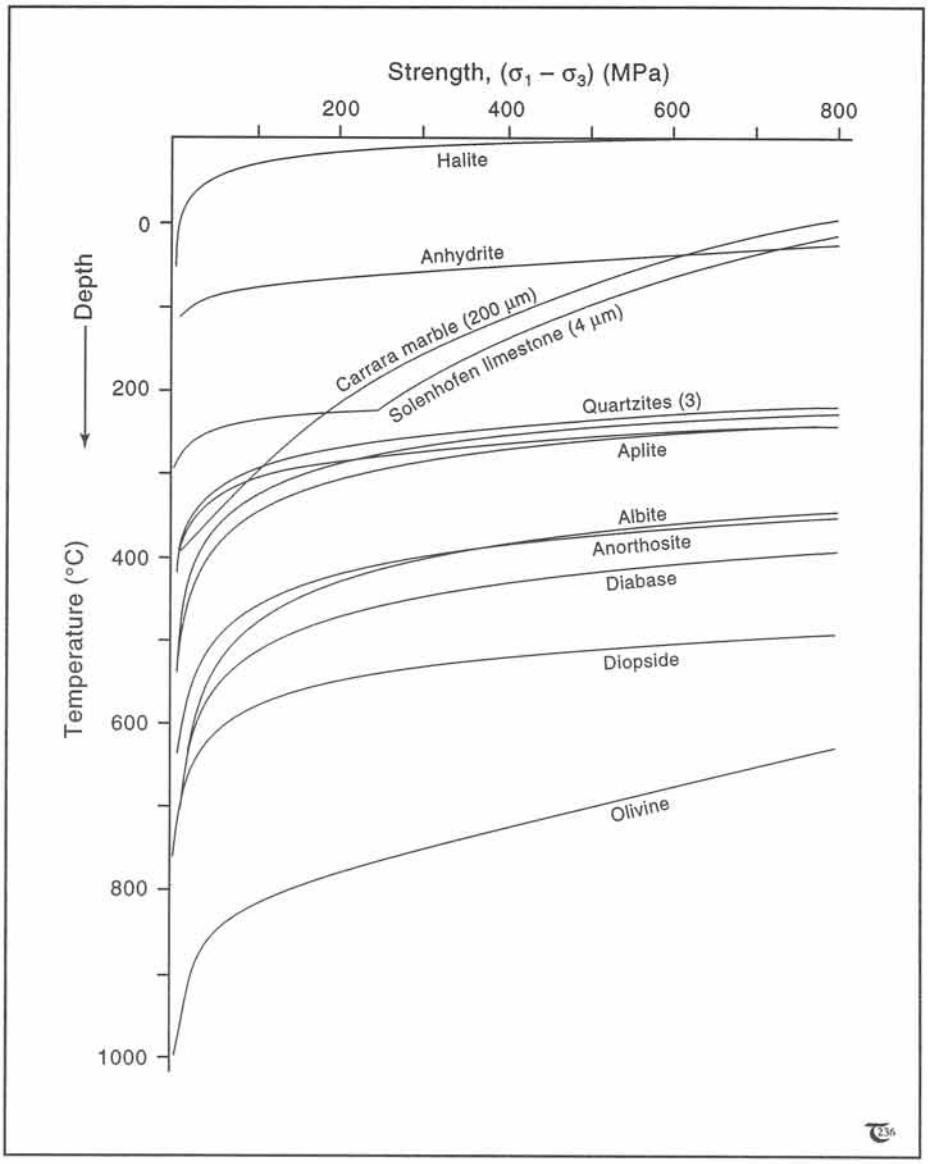

Figure 8-12: *Temperature or depth dependence of viscous strength in ductile creep for a range of rocks and minerals, depending at a constant strain-rate of 10^{-14} s^{-1}.*

8-9 Lithospheric strength profiles

The rheological data, obtained from laboratory tests on the mechanics of cold and hot rocks, can be summarized in so-called *crustal or lithospheric strength profiles* (Figs. 8-13a to c). In summary, crustal strength profiles illustrate, approximately, which portions of the crust behave in brittle and ductile fashions. This type of diagram was first used by Goetze and Evans in 1978, using Byerlee's law for the brittle regime and the flow law for solid-state creep for the ductile regime. The shallow sections of the crusts in Figures 8-13a to c have strengths as determined by Byerlee's law. The frictional resistance is very sensitive to pore water pressure, and differences in pore pressure have been incorporated in shallower parts of the crustal strength profiles of Figures 8-13a to c. The assumption of a pre-fractured crust is essential to such diagrams, in accordance with Byerlee's experimental conditions (sections 3-3 & 6-7).

The deeper, ductile section of the crustal strength profile assumes that the crustal rocks, here taken to be principally quartzitic, flow by ductile creep with a temperature-dependent strength, as determined in Figure 8-12. The depth

of the *brittle-ductile transition* in Figures 8-13a to c is determined by the intersection of the brittle and ductile strength envelopes. An increase in pore pressure increases the slope of the brittle strength envelope and, therefore, brings the brittle-ductile transition to deeper levels. An increased geothermal gradient brings the ductile creep curves to shallower levels and, therefore, also, the brittle-ductile transition. In contrast, an increase in strain-rate brings the ductile creep curve to deeper levels and, therefore, would increase the depth of brittle-ductile transition. The plots in Figures 8-13a to c assume a constant strain-rate of 10^{-14} s^{-1}.

□Exercise 8-11: Figure 8-14 shows geothermal contours for a sedimentary basin, still deforming at present. Assume that the subsurface is made up of wet quartzite with hydrostatic pore pressure. Consult Figures 8-13a & b to answer the following questions. a) How deep does one need to drill before the first ductile deformation structures can be expected in locations A and B, respectively? b) What would be the depths if the rocks turn out to be dry?

The maximum stress possible in the crustal sections of Figures 8-13a to c occurs at the depth of brittle-ductile transition. Larger stresses cannot occur within the rock, because such stresses would be relieved, either by ductile creep or by brittle faulting, depending upon the depth of deformation. The dominant deformation mecha-

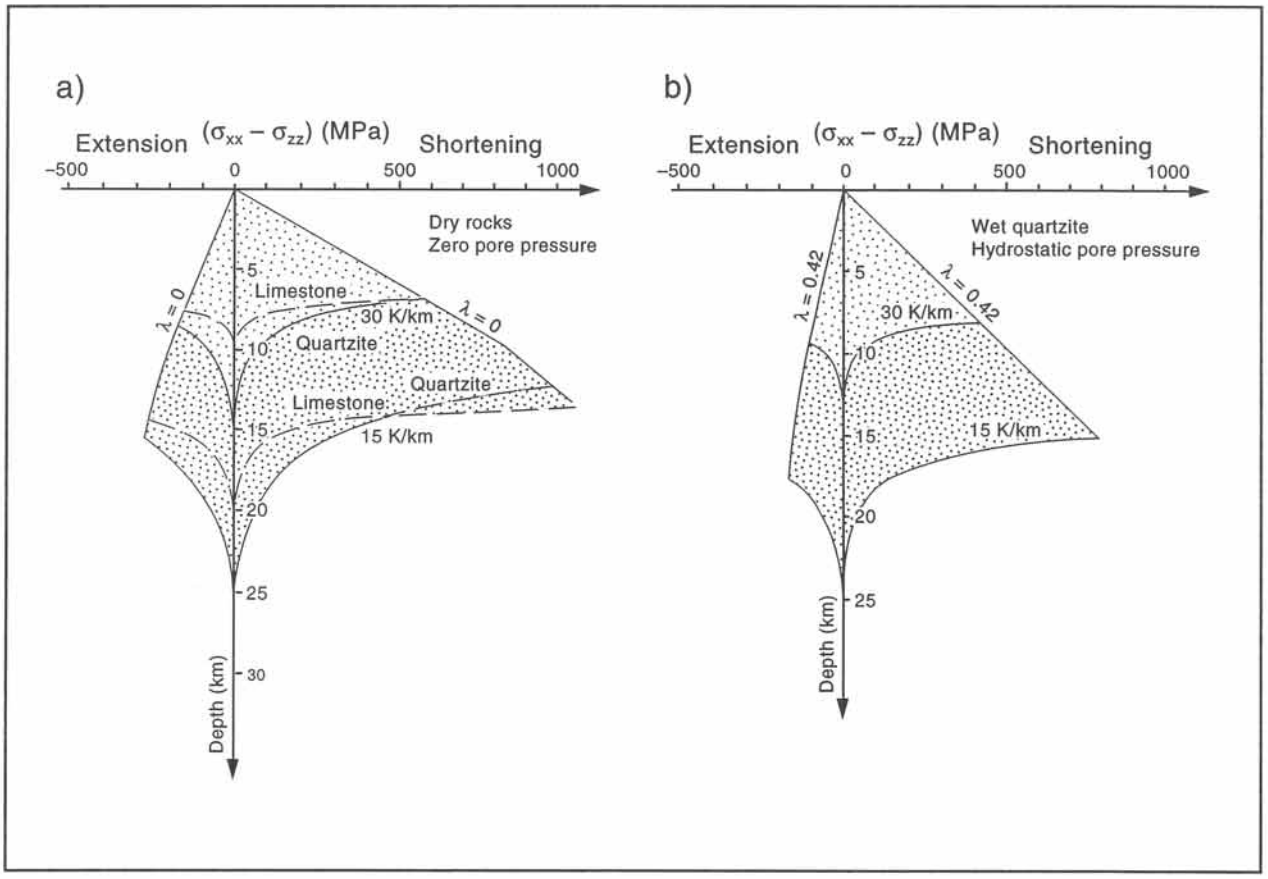

Figure 8-13a & b: *Crustal strength profiles for: (a) dry rocks, and (b) rocks with hydrostatic pore pressure.*

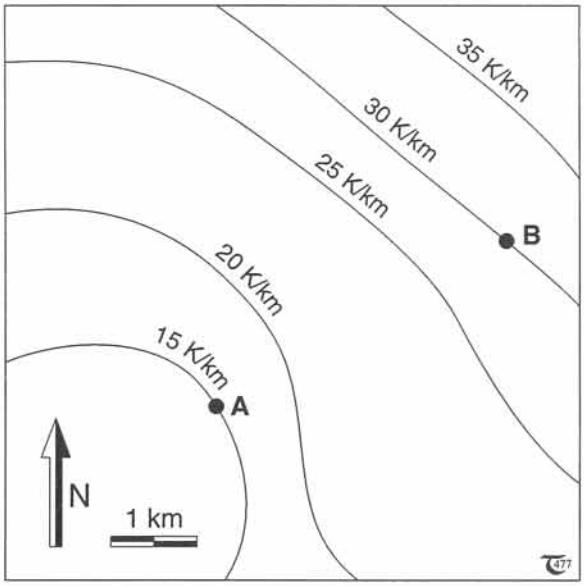

Figure 8-14: Geothermal gradient map, showing borehole locations A and B of exercise 8-11.

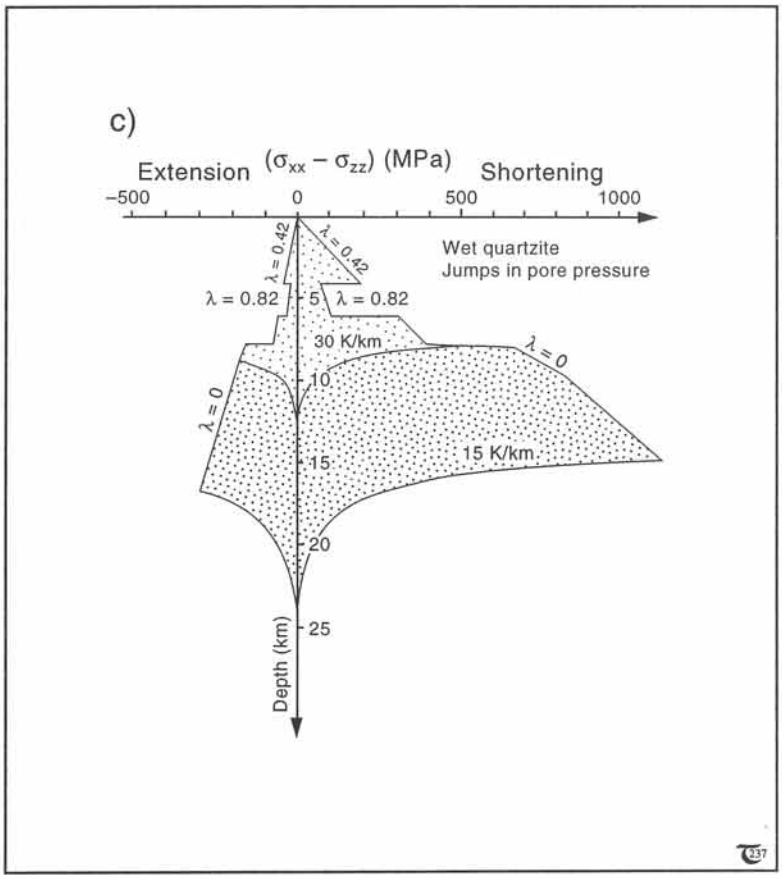

Figure 8-13c: Crustal strength profile for rocks with jumps in pore pressure.

nism (requiring the least deviatoric stress for activation) at shallow depths is brittle faulting (frictional plastic slip). This is true simply because the deviatoric stress cannot attain the magnitude required to activate flow by crystalline creep, as such stress is first relieved by frictional slip. Reversely, the dominant deformation mechanism in the deeper crust is ductile creep, because the deviatoric stresses required there are lower than those required to activate fault movement.

8-10 Depth of brittle-ductile transition

The depth of brittle-ductile transition will be different for different lithologies, because the position of the ductile-creep curve is shifting for each particular rock type. Figure 8-15 illustrates the generalized rheological structure of the crust and the upper mantle. The crustal portion of the lithosphere is taken to be principally composed of quartz. The brittle-ductile transition lies at about 15 kilometers' depth, coinciding with the separation between the upper and lower crust, depending upon the local geothermal gradient. The mantle portion of the mechanically strong part of the lithosphere (MSL) is principally composed of olivine. The depth of the brittle-ductile transition in the upper mantle is, therefore, determined by the position of the ductile creep curve for olivine, which intersects the brittle strength envelope at 35 km depth.

The model of Figure 8-15 explains why the seismic activity generated on fault-slip planes is largely concentrated in the upper crust and upper mantle. Normally, the lower crust and deeper mantle deform by ductile creep, and faulting cannot occur there, thus precluding any earthquakes. Deep earthquakes, originating from the lower mantle, are thought to be generated within relatively cold slabs of oceanic litho-

sphere sunk into the mantle. The strength of the lower crust is rapidly decreasing towards the crust-mantle boundary. This fact features centrally in so-called *delamination models*, in which it is hypothesized that the crust separates from the mantle part of the lithosphere in plate collisions.

The local physical conditions actually determine the shape of the crustal strength profile by variations in the pore water pressure (which affects Byerlee's law) and the crustal thickness (which affects the local heat flow and thus the geothermal gradient, controlling the viscosity profile). The crust of ancient cratons is unusually thick, as can be seen from a deep MOHO, determined by seismic reflection profiling and the global heat flow map. This implies that the deeper parts of Precambrian shields are cold and

☐Exercise 8-12: a) Draw the lithospheric strength profiles for a Precambrian shield area with a 40 km deep MOHO and geothermal gradient of 15 K per km, as well as a strength profile for the adjacent continental margin sequence with a 25 km deep MOHO and gradient of 30 K per km. b) Explain why the margin deforms much faster than the Precambrian interior.

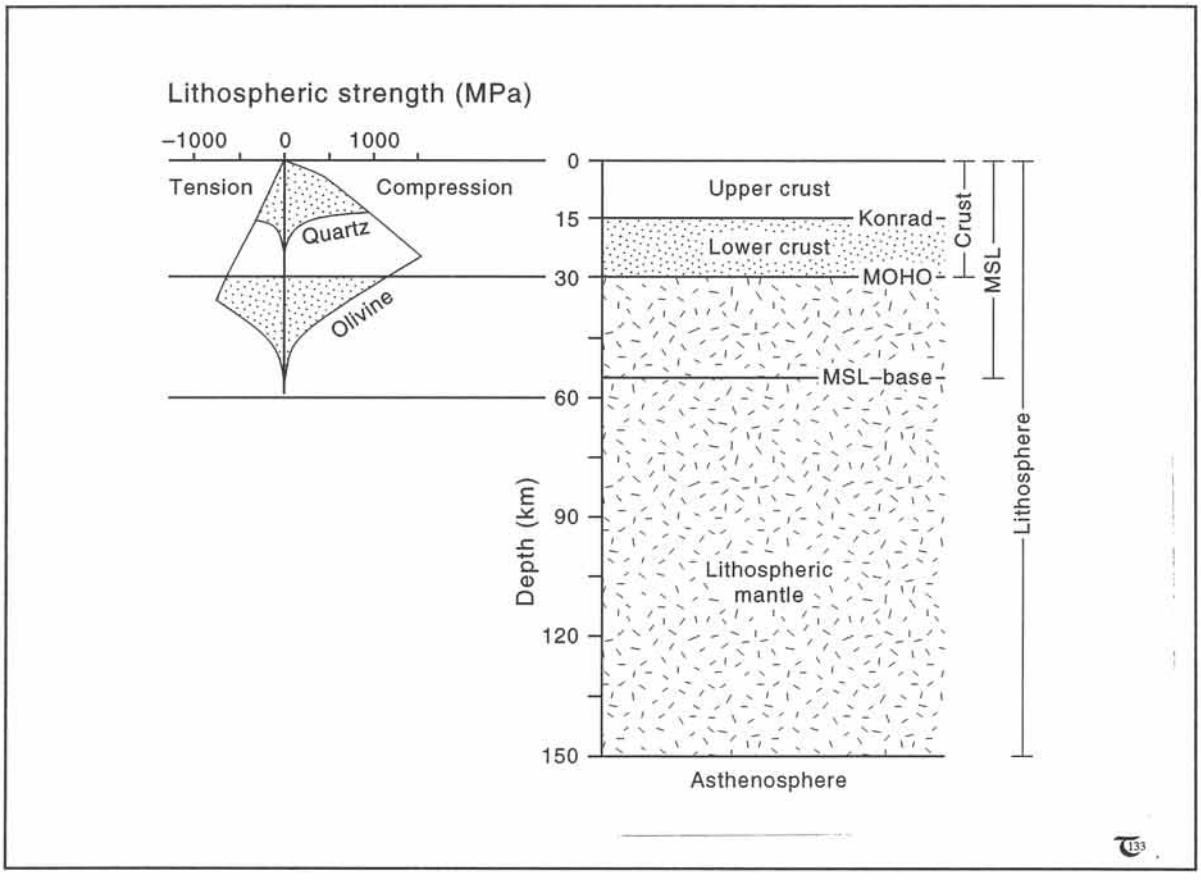

Figure 8-15: *Idealized section of the lithosphere, distinguishing a mechanically strong lithosphere (MSL), upper and lower crust (Konrad discontinuity) and Mohorovicic discontinuity at the base of the crust. The generalized strength of the MSL is shown in the lithospheric strength profile.*

☐Exercise 8-13: Figure 8-16 illustrates a deep seismic reflection profile across northern Scotland. The crustal layers 1 and 2 are extended by normal faults, mostly curving into a sole thrust at the top of layer 1. The Outer Isle Fault (OIF) soles out at the base of layer 1. The heat flow increases in the direction of the upper plate. Use the crustal strength profiles, included in Figure 8-16, to explain the fault patterns seen in the seismic section.

brittle at depths where other continental crust would exhibit ductile behavior. Old cratons remain largely undeformed in modern times just because relatively cold cratonic crust gives them an overall rheological signature stiffer than that of the adjacent non-cratonic areas of the continents.

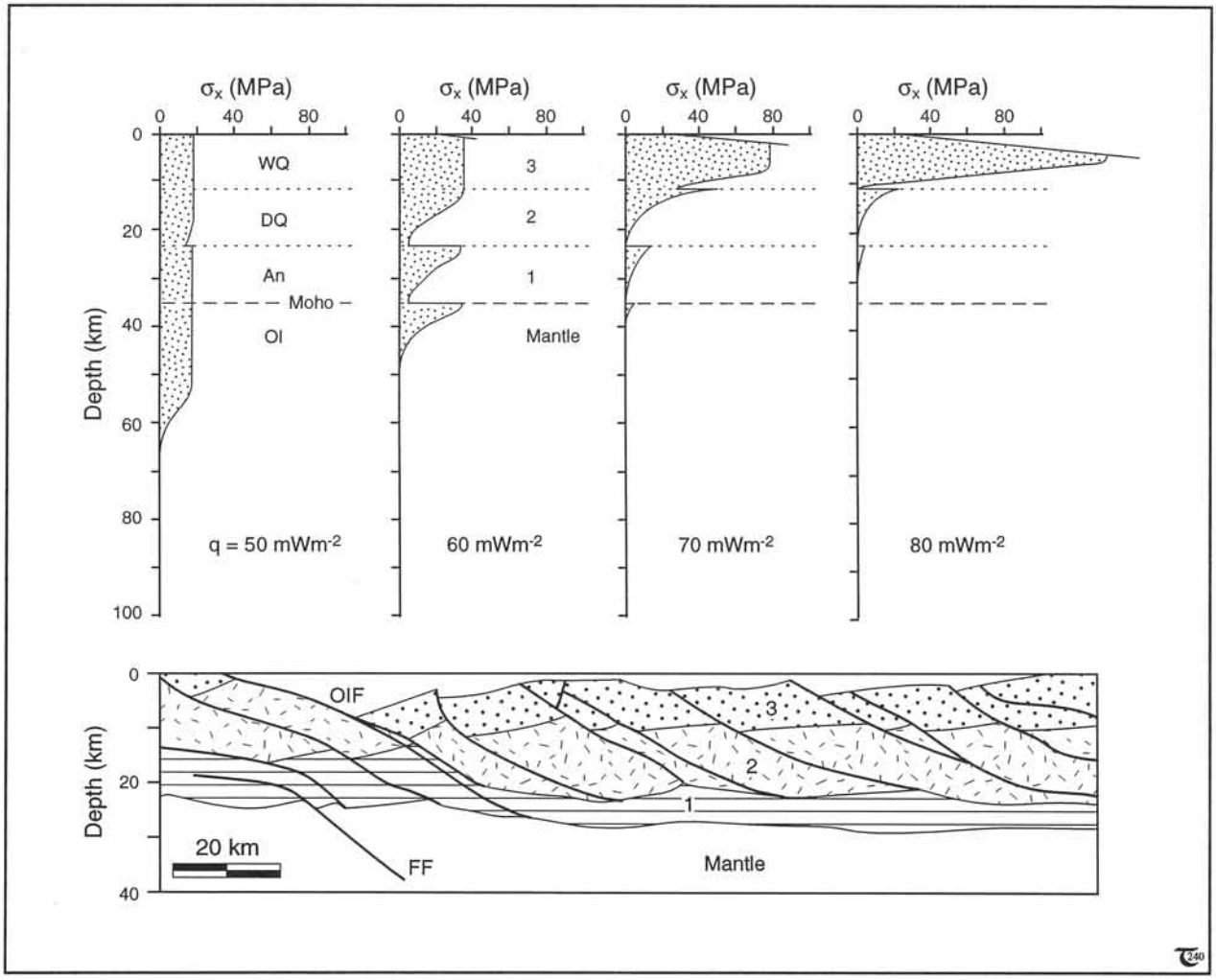

Figure 8-16: *Crustal section across northern Scotland. The crust is subdivided into: (1) granulite facies rocks (anorthosites), (2) Lewisian gneisses (dry quartz), and (3) Caledonian metamorphic rocks (wet quartz), overlaid by unornamented Torridonian to Mesozoic sedimentary rocks. Also shown are the Flannan Fault (FF) and Outer Isles Fault (OIF). See exercise 8-13.*

References

A. Books

Viscosity and Flow Measurement (1963, Interscience Publishers, 406 pages), by J.R. van Wazer, J.W. Lyons, K.Y. Kim, and R.E. Colwell. This is a very instructive text by chemical engineers familiar with polymer rheology and the instruments used to measure polymer viscosity.

Rheology of the Earth (1987, Allen & Unwin, 366 pages), by Giorgio Ranalli. This is a comprehensive text on deformation and flow processes in geophysics and geodynamics. The approach is quantitative throughout, but it is well-explained and applied to practical situations.

An Introduction to Rheology (1989, Elsevier, 199 pages), by H.A. Barnes and J.F. Hutton. This is a somewhat specialized text by chemical engineers, concentrating on the rheology of viscous and visco-elastic substances.

B. Articles

Some key references to creep laws for common rocks and minerals and their application in lithospheric strength profiles are listed below:

Brace, W.F. and Kohlstedt, D.L. (1980, *Journal of Geophysical Research*, volume 85, pages 6,248 to 6,252). Limits on lithospheric stress, imposed by laboratory experiments.

Carter, N.L. (1976, *Reviews of Geophysics and Space Physics*, volume 14, pages 301 to 360). Steady-state flow in rocks.

Carter, N.L. and Hansen, F.D. (1983, *Tectonophysics*, volume 92, pages 275 to 333). Creep of rock salt.

Carter, N.L. and Tsenn, M.C. (1987, *Tectonophysics*, volume 136, pages 27 to 63). Flow properties of continental lithosphere.

Goetze, C. and Evans, B. (1979, *Geophysical Journal Royal Astronomical Society*, volume 59, pages 463 to 478). Stress and temperature in the bending lithosphere, as constrained by experimental rock mechanics.

Joffé, A.F. and Lewitsky, M.A. (1925, *Zeitschrift für Physik*, volume 31, pages 576 to 583). Über die Festigkeit und Elastizitätsgrenze des Natürlichen Steinsalzes.

Kirby, S.H. (1980, *Journal of Geophysical Research*, volume 85, pages 6,353 to 6,363). Tectonic stress in the lithosphere: constraints provided by the experimental deformation of rocks.

Kirby, S.H. (1983, *Reviews of Geophysics and Space Physics*, volume 21, pages 1,458 to 1,487). Rheology of the lithosphere.

Kirby, S.H. and Kronenberg, A.K. (1987, *Reviews of Geophysics*, volume 25, pages 1,219 to 1,244). Rheology of the lithosphere: selected topics.

Spiers, C.J., Urai, J.L., Lister, G.S., Boland, J.N., and Zwart, H.J. (1986, *Commission of the European Communities, Nuclear Science and Technology, Final Report, EUR 10399 EN*, 131 pages). The influence of fluid-rock interaction on the rheology of salt rock.

Urai, J.L., Spiers, C.J., Zwart, H.J., and Lister, G.S. (1986, *Nature*, volume 324, page 557). Weakening of rock salt by water, during long-term creep.

The rheology of polymers and conditions for their rheological similarity to rock creep for dynamic modeling purposes have been discussed in the following papers by the author:

Weijermars, R. (1986a, *Applied Physics Letters*, volume 48, pages 109 to 111). Polydimethylsiloxane flow defined for experiments in fluid dynamics.

Weijermars, R. (1986b, *Naturwissenschaften*, volume 73, pages 33 to 34). Finite strain of laminar flows can be visualized in SGM36-polymer.

Weijermars, R. (1986c, *Tectonophysics*, volume 124, pages 325 to 358). Flow behavior and physical chemistry of Bouncing Putties and related polymers in view of tectonic laboratory applications.

Weijermars, R. and Schmeling, H. (1986, *Physics of the Earth and Planetary Interiors*, volume 43, pages 316 to 330). Scaling of Newtonian and non-Newtonian fluid dynamics without inertia for quantitative modeling of rock flow due to gravity (including the concept of rheological similarity).

Weijermars, R., Jackson, M.P.A., and Vendeville, B. (1993, *Tectonophysics*, volume 217, pages 143 to 174). Rheological and tectonic modeling of salt provinces.